1-1-2020

Decrease in 230Th in the Amundsen Basin since 2007: Far-field effect of increased scavenging on the shelf?

Ole Valk

Michiel M. Rutgers Van Der Loeff

Walter Geibert

Sandra Gdaniec

S. Bradley Moran

See next page for additional authors

10.5194/os-16-221-2020

Valk, O., Rutgers van der Loeff, M. M., Geibert, W., Gdaniec, S., Moran, S. B., Lepore, K., ... & Paffrath, R. (2020). Decrease in 230Th in the Amundsen Basin since 2007: far-field effect of increased scavenging on the shelf?. *Ocean Science, 16*, 221-234. https://doi.org/10.5194/os-16-221-2020

Ocean Sci., 16, 221–234, 2020
https://doi.org/10.5194/os-16-221-2020

Ocean Science Open Access EGU

Decrease in ^{230}Th in the Amundsen Basin since 2007: far-field effect of increased scavenging on the shelf?

Ole Valk[1], Michiel M. Rutgers van der Loeff[1], Walter Geibert[1], Sandra Gdaniec[2], S. Bradley Moran[3], Kate Lepore[4], Robert Lawrence Edwards[5], Yanbin Lu[6], Viena Puigcorbé[7], Nuria Casacuberta[8,9], Ronja Paffrath[10], William Smethie[11], and Matthieu Roy-Barman[12]

[1]Alfred Wegener Institute Helmholtz Centre for Polar and Marine Research, 27570 Bremerhaven, Germany
[2]Department of Geological Sciences, Stockholm University, 106 91, Stockholm, Sweden
[3]College of Fisheries and Ocean Sciences, University of Alaska Fairbanks, Fairbanks, AK 99775, USA
[4]Department of Astronomy, Mount Holyoke College, South Hadley, MA 01075, USA
[5]Department of Earth and Environmental Sciences, University of Minnesota, Minneapolis, MN 55455, USA
[6]Earth Observatory of Singapore, Nanyang Technological University, Singapore 639798, Singapore
[7]Center for Marine Ecosystem Research, School of Science, Edith Cowan University, Joondalup, WA 6027, Australia
[8]Laboratory of Ion Beam Physics, ETH Zurich, 8093 Zurich, Switzerland
[9]Institute of Biogeochemistry and Pollutant Dynamics, Environmental Physics, ETH Zurich, 8092 Zurich, Switzerland
[10]Max Planck Research Group for Marine Isotope Geochemistry, Institute for Chemistry and Biology of the Marine Environment, University of Oldenburg, 26129 Oldenburg, Germany
[11]Lamont-Doherty Earth Observatory, Palisades, NY 10964-8000, USA
[12]Laboratoire des Sciences du Climat et de l'Environnement, LSCE/IPSL, CEA – CNRS – UVSQ, Université Paris-Saclay, 91191 Gif-sur-Yvette, France

Correspondence: Ole Valk (ole.valk@awi.de)

Received: 8 May 2019 – Discussion started: 14 June 2019
Revised: 8 November 2019 – Accepted: 12 December 2019 – Published: 14 February 2020

Abstract. This study provides dissolved and particulate ^{230}Th and ^{232}Th results as well as particulate ^{234}Th data collected during expeditions to the central Arctic Ocean (GEOTRACES, an international project to identify processes and quantify fluxes that control the distributions of trace elements; sections GN04 and GIPY11). Constructing a time series of dissolved ^{230}Th from 1991 to 2015 enables the identification of processes that control the temporal development of ^{230}Th distributions in the Amundsen Basin. After 2007, ^{230}Th concentrations decreased significantly over the entire water column, particularly between 300 and 1500 m. This decrease is accompanied by a circulation change, evidenced by a concomitant increase in salinity. A potentially increased inflow of water of Atlantic origin with low dissolved ^{230}Th concentrations leads to the observed depletion in dissolved ^{230}Th in the central Arctic. Because atmospherically derived tracers (chlorofluorocarbon (CFC), sulfur hexafluoride (SF_6)) do not reveal an increase in ventilation rate, it is suggested that these interior waters have undergone enhanced scavenging of Th during transit from Fram Strait and the Barents Sea to the central Amundsen Basin. The ^{230}Th depletion propagates downward in the water column by settling particles and reversible scavenging.

1 Introduction

The Arctic Ocean is one of the most rapidly changing parts of the Earth's ocean–atmosphere system as a result of climate change. Underlying the potential anthropogenic changes is a large natural variability in the Arctic. Due to the limited observations in this extreme environment, establishing datasets that allow an assessment of its variability is important. Natural tracers of physical, chemical and biological processes provide an integrated description of the changing state of the system. They are therefore key tools to investigate processes,

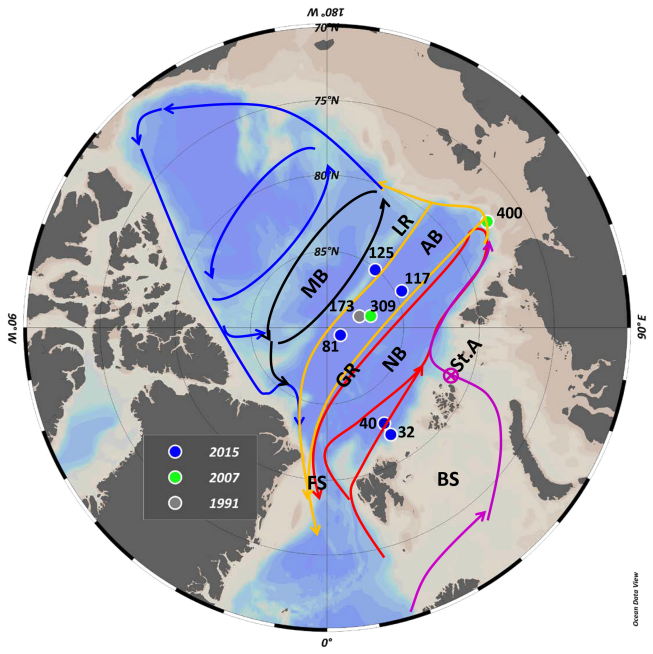

Figure 1. Map of the Arctic Ocean and station overview. AB: Amundsen Basin; NB: Nansen Basin; GR: Gakkel Ridge; MB: Makarov Basin. BS: Barents Sea; FS: Fram Strait; LR: Lomonosov Ridge; St.A: St. Anna Trough with intermediate water circulation patterns after Rudels (2009). Red is the Atlantic inflow through Fram Strait (FSBW) and return flow through the Nansen Basin; purple is the inflow through the Barents Sea (BSBW). Atlantic layer circulation in the Amundsen Basin (orange), the Makarov Basin (black) and Canada Basin (blue) are indicated as arrows. Copyright: Schlitzer (2018).

monitor environmental changes and provide an observational baseline against which models can be tested.

1.1 Hydrography and circulation patterns of the central Arctic Ocean

The central Arctic Ocean is divided into the Amerasian Basin and Eurasian Basin by the Lomonosov Ridge (Fig. 1). The Gakkel Ridge separates the Eurasian Basin further into the Nansen Basin and the Amundsen Basin, while the Amerasian Basin is separated into the Makarov and Canada basins by the Alpha–Mendeleev Ridge.

Water masses of the Arctic Ocean are commonly distinguished as five layers (Rudels, 2009). The uppermost low-salinity Polar Mixed Layer (PML) varies in thickness between winter and summer due to melting and freezing of sea ice. Salinity ranges from 30 to 32.5 (Amerasian Basin) to 32–34 (Eurasian Basin). Below the PML is a 100–250 m thick halocline in which salinity increases sharply from approximately 32.5 to 34.5. The underlying Atlantic Layer is characterized in salinity and temperature by waters of Atlantic origin and is usually found between 400 and 700 m water depth. Its salinity is 34.5–35. Intermediate waters down to 1500 m, with a salinity of 34.87–34.92, are still able to exchange over the Lomonosov Ridge. In contrast, deep and bottom waters differ between the Eurasian Basin (salinity: 34.92–34.945) and the Amerasian Basin (salinity: 34.92–34.96) due to the topographic barrier.

Atlantic waters from the Norwegian Atlantic Current enter the Arctic Ocean via Fram Strait and the Barents Sea. Fram Strait Branch Water (FSBW) is supplied through the West Spitsbergen Current (WSC) (Rudels, 2012) (Fig. 1). Barents Sea Branch Water (BSBW) enters through the Barents Sea and consists of Atlantic water that undergoes strong modifications in the Barents and Kara seas by cooling down and mixing with continental runoff and meltwater (Rudels et al., 2015). The BSBW enters the Nansen Basin through the St. Anna Trough, where limited mixing with the FSBW occurs. Once in the polar ocean, surface waters follow wind-driven ice motion (Aagaard et al., 1980), whereas deeper Atlantic water branches (FSBW and BSBW) flow cyclonically to the east, forming a boundary current along the continental slopes of the Nansen and Amundsen basins.

BSBW (approx. 1025 m depth; Tanhua, 2009) and FSBW (approx. 425 m) return in the Atlantic and intermediate water layers along the Lomonosov Ridge towards Fram Strait (Rudels et al., 2013) (Fig. 1), and a second branch crosses the Lomonosov Ridge entering the Canada Basin following the Arctic Ocean Boundary Current (AOBC) (Rudels, 2009).

Deep waters of the Arctic Ocean have similar structure, with a thick intermediate layer stratified in temperature but with salinity almost constant with depth (Rudels, 2009). Yet, the Amerasian Basin Deep Water is warmer, saltier and less dense than the Eurasian Basin Deep Water (EBDW) (Aagaard, 1981; Worthington, 1953). The deepest exchange of Makarov Basin water, part of the Amerasian Basin, with Eurasian Basin water occurs through a depression of the ridge, called the Intra-Basin with a sill depth of approximately 1800 m (Björk et al., 2007, 2010; Jones et al., 1995). Water from the Amundsen Basin flows over the Lomonosov Ridge into the deep Makarov Basin and in the reverse direction (Middag et al., 2009).

Another important component of the Arctic Ocean is the freshwater content, coming from the melting of sea ice and from river runoff. The fresh water content of the central Arctic Ocean is currently at the highest level since the early 1980s and is expected to increase in the future (Rabe et al., 2014), which could lead to a stronger stratification of the water column. This process is supported by sea ice decline, as observed in the Beaufort Gyre (Wang et al., 2018). Karcher et al. (2012) suggest a reversal in flow direction of Atlantic Water in the Canada Basin at intermediate water depths on the basis of ^{129}I observations and modelling. This could lead to a decoupling of flow regimes in the Canada and Eurasian basins and reduce exchange times between the two major basins of the Arctic Ocean (Karcher et al., 2012).

1.2 Particle fluxes, shelf input and biological productivity

Biological productivity in the central Arctic Ocean and related particle fluxes are lower than in other oceans due to the perennial sea ice cover (Clark and Hanson, 1983). This is expected to change in the future when light limitation is relieved by sea ice retreat (Pabi et al., 2008). Arctic sea ice extent is declining (Serreze et al., 2016) and ice is becoming thinner (Serreze and Stroeve, 2015). Biological productivity may increase and begin earlier in the year, at least in the Pacific part of the Arctic, depending on nutrient supply (Hill et al., 2017). Recent studies show that productivity is still low in the central Arctic Ocean, limited by both light and nutrient availability (Arrigo and van Dijken, 2015). Highest net community production (NCP) is found at the ice edge of the Nansen Basin and over the shelves, while the Amundsen Basin shows the lowest NCP (Ulfsbo et al., 2014). Apart from the possible effect on NCP, the declining sea ice cover will also enhance ice-derived particle fluxes (Arrigo et al., 2008; Boetius et al., 2013). The Arctic Ocean has the largest relative proportion of shelves of all the World Ocean: approximately 50 % of area in total (Jakobsson, 2002). Shelf sediments and large volumes of riverine input add trace metals and carbon among other terrestrial components to Arctic shelf areas, some of which are transported to the central Arctic by the Transpolar Drift (TPD) (Wheeler et al., 1997; Rutgers van der Loeff et al., 2018, 1995). On the basis of an increase in ^{228}Ra supply to the interior Arctic Ocean, Kipp et al. (2018) suggested that the supply of shelf-derived materials is increasing, with a following change in trace metal, nutrient and carbon balances. Thawing permafrost and subsequent increasing coastal erosion (Günther et al., 2013) may increase terrestrial input to the central Arctic Ocean (Schuur et al., 2013, 2015).

1.3 Th as a tracer of water circulation and particle fluxes

Thorium isotopes have been extensively used to study and model physical oceanographic processes, such as advection, water mass mixing and particle flux (Bacon and Anderson, 1982; Rutgers van der Loeff and Berger, 1993; Roy-Barman, 2009; Rempfer et al., 2017). In seawater, ^{230}Th ($t_{1/2} = 75\,380$ years) is produced by the radioactive decay of dissolved ^{234}U. Without lateral transport by currents, the vertical distribution of ^{230}Th in the water column is controlled by reversible exchange with sinking particles and increases with depth (Bacon and Anderson, 1982; Nozaki et al., 1981). Deviations from a linear increase with a depth profile of ^{230}Th (Bacon and Anderson, 1982) suggest that oceanic currents transport ^{230}Th away from the production area or that ventilation, upwelling or depth-dependent scavenging processes play a role in the ^{230}Th distribution in the water column (e.g. Rutgers van der Loeff and Berger, 1993; Moran et al., 1995; Roy-Barman, 2009).

^{232}Th ($t_{1/2} = 1.405 \times 10^{10}$ years) is known as a tracer for shelf- or continentally derived signatures (Hsieh et al., 2011), while ^{234}Th ($t_{1/2} = 24.1$ d) serves as a tracer for particle flux (Moran and Smith, 2000).

^{230}Th in the Arctic Ocean

Several studies have addressed the regional distribution of dissolved ^{230}Th in the Arctic Ocean in relation to particle fluxes and water mass residence time over the past decades. Yet several key points to understand the removal processes of dissolved ^{230}Th are not entirely understood and the sensitivity of dissolved ^{230}Th to environmental changes is still not explained sufficiently. Bacon et al. (1989) hypothesized that the scavenging of reactive elements in the central Arctic Ocean was significantly lower than in other parts of the world to explain the high ^{230}Th concentrations observed at the Alpha Ridge and the northern Makarov Basin (Bacon et al., 1989). Edmonds et al. (1998), later confirmed by Trimble et al. (2004), showed that ^{230}Th activities in the deep southern Canada Basin were much lower, and residence times correspondingly shorter, than observed by Bacon et al. (1989) at the Alpha Ridge.

Cochran et al. (1995) calculated residence times of dissolved ^{230}Th of 18–19 years in the central Nansen Basin and 10–12 years on the Barents Sea slope. ^{230}Th concentrations in the Nansen Basin were found to be lower than those from the Alpha Ridge reported by Bacon et al. (1989), and deep water in the central Nansen Basin had lower particulate and higher dissolved ^{230}Th concentrations than near the slopes (Cochran et al., 1995). Scholten et al. (1995) found that the shallower EBDW is influenced by ventilation, in contrast to the deeper Eurasian Basin Bottom Water (EBBW) and suggested resuspension as the cause for the increased scavenging rates in the EBBW. Valk et al. (2018a) showed that the deep Nansen Basin is influenced by volcanic and hydrothermal inputs that lead to scavenging removal of ^{230}Th over several years, at least episodically.

Sedimentary $^{231}Pa_{xs}/^{230}Th_{xs}$ from the Canada Basin provided new insights into the relevance of scavenging removal and the horizontal redistribution of these tracers as well as the fractionation between the low-productivity, sea-ice-covered interior basins and the seasonally high particle flux areas at the margins. Low surface sediment $^{231}Pa_{xs}/^{230}Th_{xs}$ ratios were interpreted as a result of chemical fractionation of ^{230}Th and ^{231}Pa in the water column, resulting in preferred ^{231}Pa export out of the Arctic. Almost all of the ^{230}Th produced in situ (ca. 90 %) was estimated to be removed within the Arctic by scavenging onto particles (Moran et al., 2005), while Hoffmann et al. (2013) suggested that the deep waters of the Arctic are exchanged through Fram Strait on centennial timescales.

Roy-Barman (2009) presented a boundary scavenging profile model, showing that linear ^{230}Th concentration profiles do not necessarily imply that circulation is negligible. They suggested that the difference between the Arctic and other oceans is a considerable lateral transport of ^{230}Th from the interior to the margins.

1.4 Motivation

Global warming is triggering profound changes in the ocean, and the Arctic Ocean is especially vulnerable to such environmental forcing. Summer ice cover is rapidly declining, while the supply of terrestrial material (Günther et al., 2013) and particle flux (Boetius et al., 2013) increases and ocean circulation is changing (Karcher et al., 2012). These developments are expected to leave an imprint on the distribution of particle-reactive radionuclides, such as Th isotopes. A central motivation for this GEOTRACES study is to use the Th isotopes to depict changes in circulation and particle fluxes in the Arctic Ocean from 1991 to 2015. The basis of this study is a time series consisting of natural radionuclide data from various previous studies, combined with new data from 2007 and 2015.

2 Methods

2.1 Sampling and analysis of Th in samples collected in 2007

Sea water samples were filtered directly from the 24 L CTD (conductivity–temperature–depth) Niskin® bottles into acid-cleaned Cubitainer® containers (low-density polyethylene (LDPE)) using 0.45 µm pore size Acropaks®. Samples were collected in volumes of 1, 2 and 10 L and acidified with concentrated ultraclean HNO_3. Samples for the analysis of total ^{230}Th were taken without filtration. Analyses were performed at the University of Minnesota, Minneapolis, following methods from Shen et al. (2003). Measurements were done using inductively coupled plasma mass spectrometry (ICP-MS; Thermo Finnigan, Neptune) equipped with a secondary electron multiplier (SEM) and a retarding potential quadrupole (RPQ) energy filter.

2.2 Sampling and analysis of dissolved Th samples collected in 2015

Samples were filtered directly from the 24 L CTD Niskin® bottles into Cubitainer® containers (LDPE) through 0.45 µm pore size Acropaks® in volumes of 10 L (> 2000 m) and 20 L (< 2000 m), according to the expected concentrations (Nozaki et al., 1981). Acropaks® were used for half of the cruise and then replaced by new ones. Subsequently water samples were acidified to a pH of 1.5–2 by the addition of 1 mL acid L^{-1} (seawater) of concentrated double-distilled HNO_3.

Preconcentration and analysis of ^{230}Th and ^{232}Th were performed following GEOTRACES methods in clean laboratories of the Alfred Wegener Institute (AWI) (Anderson et al., 2012).

Samples were spiked with ^{229}Th and ^{236}U, calibrated against the reference standard material UREM11, a material in radioactive equilibrium (Hansen and Ring, 1983), followed by the addition of a purified Fe carrier solution ($FeCl_3$). The next day, the pH of the samples was raised to 8.5 by adding double-distilled NH_4OH to induce $Fe(OH)_3$ precipitation. After 72 h, when the $Fe(OH)_3$ had settled to the bottom of the Cubitainer®, the precipitate was transferred from the Cubitainer® containers to acid-cleaned 1 L Teflon® bottles, after syphoning off the supernatant water. After the dissolution of the sample in concentrated HCl, the pH was raised again to 8.5 to allow the $Fe(OH)_3$ precipitate and settle. The supernatant water was syphoned off and the precipitate was transferred into acid-cleaned 50 mL Falcon® tubes the following day. The samples were then washed by centrifugation four times at 4000 rpm for 12 min, where the supernatant was decanted before the addition of new ultrapure Milli-Q® water. Finally, the precipitation was dissolved in concentrated HCl and evaporated to a drop (> 10 µL) in an acid-cleaned 15 mL Savillex® beaker. After evaporation, the fractions of Pa, Th, U and Nd were separated using chromatographic columns filled with anion exchange resin (AG1X8, 100–200 mesh) according to GEOTRACES methods (Anderson et al., 2012). All fractions were collected in acid-cleaned 15 mL Savillex® beakers, and columns were washed and conditioned before the samples were loaded onto the columns using concentrated HCl and HNO_3.

Procedural blanks for ^{230}Th and ^{232}Th were run with each batch of 10–15 samples. Average ^{230}Th and ^{232}Th blank corrections are 0.24 fg kg^{-1} and 0.003 pmol L^{-1}, respectively. At station 81, a sample (2000 m) was divided into two samples and resulted in different dissolved ^{232}Th concentrations, probably due to Th attached to the walls of the original cubitainer. Here, an average value considering the volumes of both parts of the divided samples was calculated.

2.3 Sampling and analysis of particulate ^{234}Th samples collected in 2015

Particulate samples were taken using in situ pumps (McLane and Challenger Oceanic). In total, 268 to 860 L seawater were pumped through a 142 mm diameter, 0.45 µm pore size Supor® (polyether sulfone) filter (Anderson et al., 2012). Filters were cut aboard for subsamples under a laminar flow hood using tweezers and scalpels. Subsamples (23 mm diameter) were dried, put on plastic mounts, covered with Mylar and aluminium foil, and directly measured by beta decay counting of ^{234}Th for at least 12 h. Six months later, background measurements were performed at the AWI in Bremerhaven.

Table 1. Parameters of the profile model adapted from Rutgers van der Loeff et al. (2018), representing transient ^{230}Th in the Amundsen Basin.

Parameter	Symbol	Value	Unit
Vertical eddy diffusion coefficient	K_z	4100	$m^2\,yr^{-1}$
Exchange time 0–1500 m with Kara Sea			
initial	t_K	∞	years
during ventilation	t_K	4	years
^{230}Th Kara Sea	$^{230}Th_K$	0	$fg\,L^{-1}$
C_p/C_d ^{230}Th*	K_{230}	0.5	–
C_p/C_d ^{234}Th*	K_{234}	0.12	–
Adsorption rate constant	k_1	1.59	yr^{-1}
Desorption rate constant	k_{-1}	3.18	yr^{-1}
Particle settling rate*	S	582	$m\,yr^{-1}$

* Valk et al. (2018a). C_p: particulate concentration; C_d: dissolved concentration.

2.4 Model

The model of Rutgers van der Loeff et al. (2018) was used to analyse the downward propagation of a ventilation signal in the Atlantic layer by settling particles and radioactive ingrowth. The ^{230}Th model is based on the reversible exchange model of Bacon and Anderson (1982) and Nozaki et al. (1981) and solved with the programming language R. We first let the ^{230}Th model run with the base parameters as given for the Amundsen Basin in Table 1 of Rutgers van der Loeff et al. (2018), but without exchange with the Kara Sea, until dissolved ^{230}Th reaches a linear steady-state profile. We then simulate a hypothetical strong ventilation of the intermediate water with ^{230}Th-depleted shelf water by introducing an exchange process down to 1500 m with a ^{230}Th-free water mass on a timescale of 4 years, which causes a rapid reduction in ^{230}Th in this upper layer. The ^{230}Th profile is determined over the full water column over time since the beginning of this ventilation. Parameter values used in the simulation are listed in Table 1.

3 Results

^{230}Th results are expressed as unsupported excess ^{230}Th ($^{230}Th_{xs}$); for simplification, hereinafter ^{230}Th refers to $^{230}Th_{xs}$. Excess corrections were done following Hayes et al. (2015). ^{230}Th concentrations are corrected for a proportion of ^{230}Th released by the dissolution of lithogenic particles. This is based on parallel measurements of ^{232}Th, considering a lithogenic ratio $^{230}Th/^{232}Th = 4.0 \times 10^{-6}\,mol\,mol^{-1}$ (Roy-Barman et al., 2009).

3.1 Dissolved ^{230}Th in 1991, 2007 and 2015

Data obtained in 1991 by Scholten et al. (1995) constitute the baseline for the time series presented in this study (Fig. 2a). Dissolved ^{230}Th activities increased with depth in the Amundsen Basin in 1991, 2007 and 2015.

Station 400 (2007), located at the south-eastern margin of the Eurasian Basin, showed lower concentrations than the open-ocean stations.

3.2 Dissolved ^{232}Th in 2007 and 2015

The concentrations of dissolved ^{232}Th from 2007 and 2015 were similar. In 2015, dissolved ^{232}Th concentrations observed in the Amundsen Basin showed a decreasing trend with depth. Surface concentrations were relatively high at station 117 ($100\,pg\,kg^{-1}$) and 125 ($> 200\,pg\,kg^{-1}$). At station 81, dissolved ^{232}Th showed a relatively constant depth distribution, where surface ^{232}Th concentrations were lower compared to station 117 and 125. At stations 125 and 117 dissolved ^{232}Th also decreased slightly with depth, with station 117 showing a mid-depth maximum at 2000 m (Fig. 2c). Values from 2007 (station 309) decreased with depth until 2500 m and then slightly increased towards 4500 m. Close to the shelf (at station 400) concentrations were lower than in the open basin in 2007.

3.3 Particulate ^{234}Th from 2015

Particulate ^{234}Th from 2015 is shown as the relative amount of particulate ^{234}Th (Fig. 2d) compared to total ^{234}Th, calculated from ^{238}U activities, assuming equilibrium of total ^{234}Th with ^{238}U in deep water (Owens et al., 2011). All profiles show rather low concentrations of particulate ^{234}Th in the Amundsen Basin. Especially below 2000 m particulate ^{234}Th is much higher in the Nansen Basin (Valk et al., 2018a).

4 Discussion

4.1 Temporal evolution of dissolved ^{230}Th in the Amundsen Basin

Figure 2a shows ^{230}Th concentrations from 2015 and the temporal development since 1991.

Temporal changes have been manifest over the entire water column since 2007. With one exception, the 2015 concentration range is below 2007 and 1991 (Scholten et al., 1995). This difference is larger than the concentration range for the three 2015 profiles (Fig. 2a). The three stations from 2015 (81, 117 and 125) are distributed over a wide area of the Amundsen Basin (Fig. 1). Because all stations show lower concentrations in 2015, this points to a temporal rather than a regional variability over the entire basin. The decrease in dissolved ^{230}Th in the Amundsen Basin started after 2007, con-

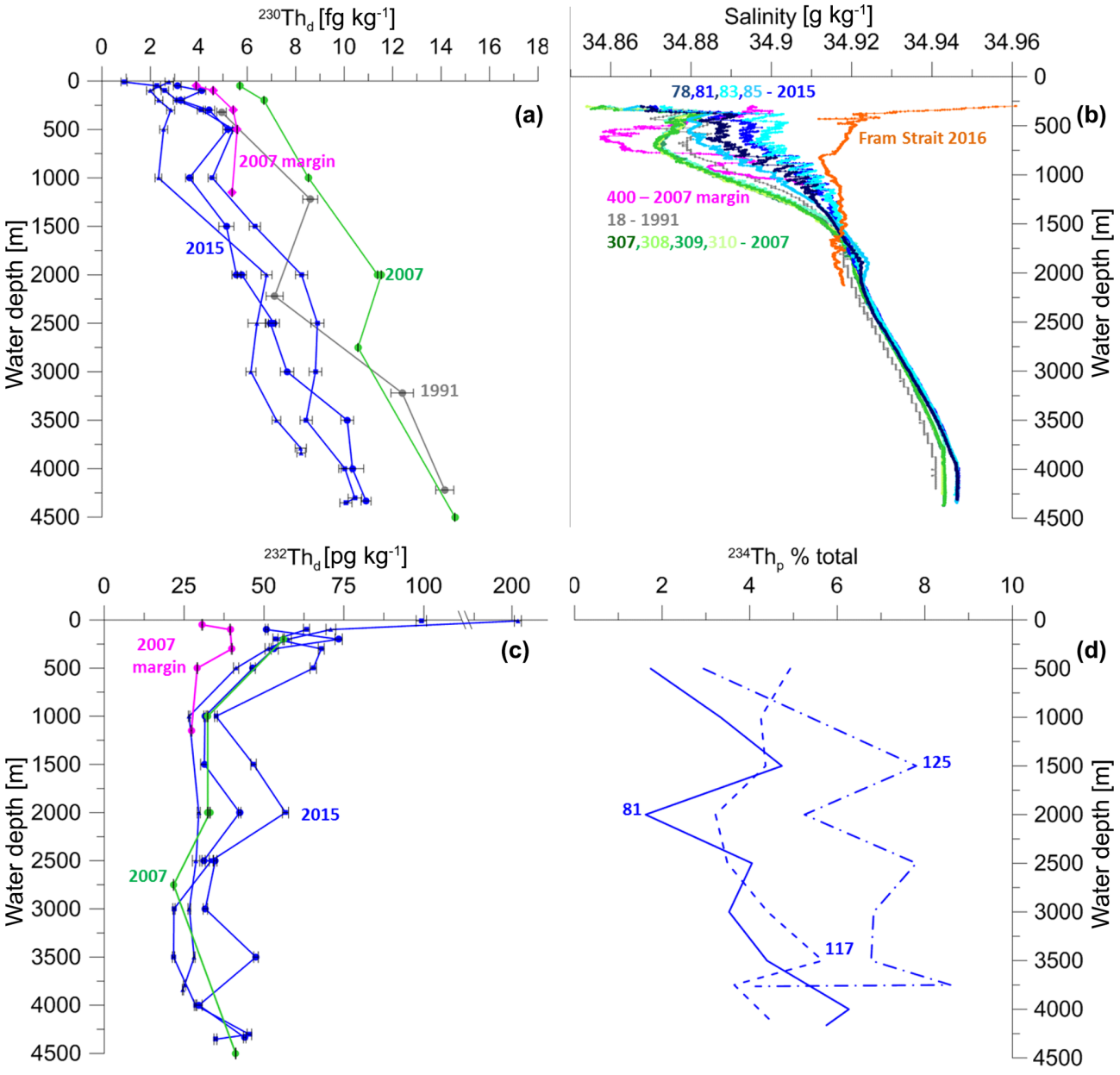

Figure 2. (a) Amundsen Basin dissolved ^{230}Th from 2015 in blue (81: dots; 117: squares; 125: triangles; same as symbols in Fig. 2a and c), 2007 in green (309), 2007 margin in pink and 1991 in grey (173). **(b)** Amundsen Basin salinity profiles from 2015 (Rabe et al., 2016), 2007 (Schauer and Wisotzki, 2010) and 1991 (Rudels, 2010) and Fram Strait from 2016 (Kanzow et al., 2017). **(c)** Dissolved ^{232}Th from 2015 (81 = dashed, 117 = dashed dotted, 125 = solid), 2007 (309 = green), and 2007 margin (400 = pink) and **(d)** particulate ^{234}Th from 2015 in percent of total ^{234}Th (81: dashed; 117: dashed–dotted; 125: solid).

sidering the similar concentrations in 1991 and 2007. Dissolved ^{230}Th decreased by 0.32 fg kg^{-1} yr^{-1} at 300–500 m water depth and by 0.52 fg^{-1} kg^{-1} yr^{-1} at 1000–1500 m. ^{230}Th is known to respond to particle fluxes as well as ocean circulation (Anderson et al., 1983b, a). A reduction in dissolved ^{230}Th concentrations can therefore be caused by either increased scavenging (Anderson et al., 1983b) or by changing circulation (Anderson et al., 1983a).

4.2 Scavenging in the central Amundsen Basin

Biological production in the central Arctic Ocean in 2011 was not higher than in 2007 (Ulfsbo et al., 2014). Therefore, enhanced biological production in the Amundsen Basin and subsequent sinking particles can be excluded as a reason for the changing Th distributions. Enhanced scavenging by lithogenic material at these stations can also be excluded because for all three stations from 2015, dissolved ^{232}Th val-

ues at 1000 m are in the same range or lower than observed in 2007 (Fig. 2c). Low dissolved ^{232}Th is taken here as an indicator of low amounts of lithogenic material. Enhanced particle loads would result in high concentrations of particulate ^{234}Th, as observed in the deep Nansen Basin where particulate ^{234}Th ranges between 3.3 % and 9.1 % of total ^{234}Th (Valk et al., 2018a). In the Amundsen Basin only station 125 (2015), located at the slope of the Lomonosov Ridge, shows relatively high values of particulate ^{234}Th in the deep water from 1500 m downward (Fig. 2d). This feature could be explained by the resuspension of slope sediments along the Lomonosov Ridge, as no increased scavenging was observed in the deep Amundsen Basin (Slagter et al., 2017). Slagter et al. (2017) argue that similar riverine surface influence of humic substances in the Amundsen Basin and in the Makarov Basin did not lead to increased scavenging at depth in the Amundsen Basin, even at stations influenced by the TPD (e.g. station 125) (Slagter et al., 2017; Rutgers van der Loeff et al., 2018). This is in contrast to the Makarov Basin, where Slagter et al. (2017) observed a slight increase in dissolved Fe-binding organic ligand concentrations and reduced dissolved Fe concentrations that may point to more intense scavenging or lower Fe inputs (Slagter et al., 2017; Klunder et al., 2012), while the high ^{232}Th observed at the surface of station 125 points to a notable continental component, a signal that is not observed below (Fig. 2c). Hence, our observations are consistent with Slagter et al. (2017). To summarize, dissolved ^{232}Th generally did not increase since 2007, except for station 117 at 2000 m and station 81 at 3500 m. Recent studies about Ra isotopes, Fe-binding ligands, NCP estimates and the particulate data (^{234}Th, ^{232}Th) do not point to enhanced particle fluxes in the central Amundsen Basin. Therefore, and putting all these different parameters together, it can be concluded that scavenging of ^{230}Th within the Amundsen Basin is unlikely to be the primary factor for the observed reduction between 2007 and 2015 in the Amundsen Basin.

4.3 At 500–1500 m: intermediate water mass changes

The decrease in dissolved ^{230}Th at depths between 500 and 1500 m for stations 81, 117 and 125 in the Amundsen Basin (2015) is most prominent at 1000 m, where concentrations decreased to half of the value in 2007 (Fig. 2a). This depth range in the Amundsen Basin is ventilated on considerably shorter timescales than in the Nansen and Makarov basins by a westward boundary circulation (Tanhua et al., 2009).

The drop in dissolved ^{230}Th at 1000 m corresponds to an increase in the ^{129}I/^{236}U ratio (Fig. 3), implying a higher Atlantic influence of younger waters (Casacuberta et al., 2018), which in turn is in agreement with an increase in the circulation or ventilation rate between 750 and 1500 m. For station 81, in the central Amundsen Basin, Rutgers van der Loeff et al. (2018) estimated a ventilation age based on SF_6 data of 15–18 years at 1000 m. This estimate fits timescales based on ^{228}Ra data and is supported independently by the

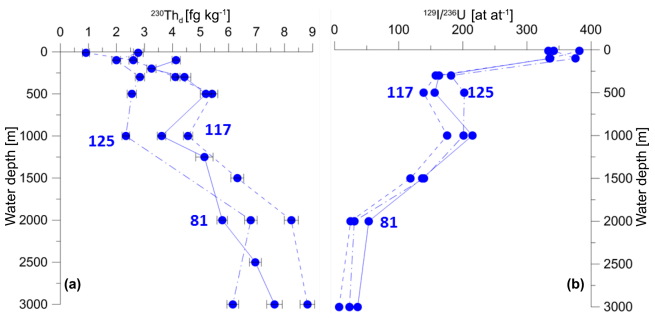

Figure 3. (a) Dissolved ^{230}Th and **(b)** ^{129}I/^{236}U (Casacuberta et al., 2018) for three stations in the Amundsen Basin, 2015.

^{129}I/^{236}U ratio (Rutgers van der Loeff et al., 2018). While anthropogenic radionuclides (Fig. 3) imply exchange with young shelf waters of Atlantic influence, it is unclear to what extent the change in ^{230}Th may be caused by exchange with the Makarov Basin. Tanhua et al. (2009) found notable changes in CFC tracer ages at the North Pole, indicating older waters in 1994 compared to 1991 and 2005 at 400 m; a change that was also documented in silicate concentrations (Tanhua et al., 2009). This feature probably reflected a shift in the front of Eurasian and Canada Basin water around the year 1994, with Canadian Basin water penetrating deeper into the central Amundsen Basin (Tanhua et al., 2009). Unfortunately, there are no ^{230}Th data from this phase of penetration of Canada Basin water around 1994. If the ^{230}Th data from 1991 are connected to CFC data from the same year, while the ^{230}Th data from 2007 are connected to CFC data of 2005 (Tanhua et al., 2009), they are both representative of periods of low intrusion of Canada Basin water over the Lomonosov Ridge. The renewed intrusion of Canada Basin water in 2015 can be excluded as mechanism for the observed change in ^{230}Th because this would increase rather than decrease dissolved ^{230}Th concentrations in the Amundsen Basin (Scholten et al., 1995; Edmonds et al., 2004; this study). Moreover, the intrusion of Canada Basin water would not match the ventilation age estimated by Rutgers van der Loeff et al. (2018), since the Canada Basin water is known to be much older than Amundsen Basin water at this depth (Tanhua et al., 2009). Hence, it is suggested that the changes in the Amundsen Basin cannot be explained by interaction with the Makarov Basin. On the contrary, salinity distributions imply that the influence of Atlantic waters in the Amundsen Basin had increased at 500–1500 m by 2015, indicating that water masses changed after 2007 (Fig. 2b). Figure 2b shows salinity profiles for three stations from the Amundsen Basin from 2007 (Schauer and Wisotzki, 2010), three from 2015 (Rabe et al., 2016), and one from 1991 (Rudels, 2010). In 2015, the intermediate waters of the Amundsen Basin had a stronger Atlantic contribution (Polyakov et al., 2017; Rabe et al., 2016). This change is correlated with the decrease in dissolved ^{230}Th.

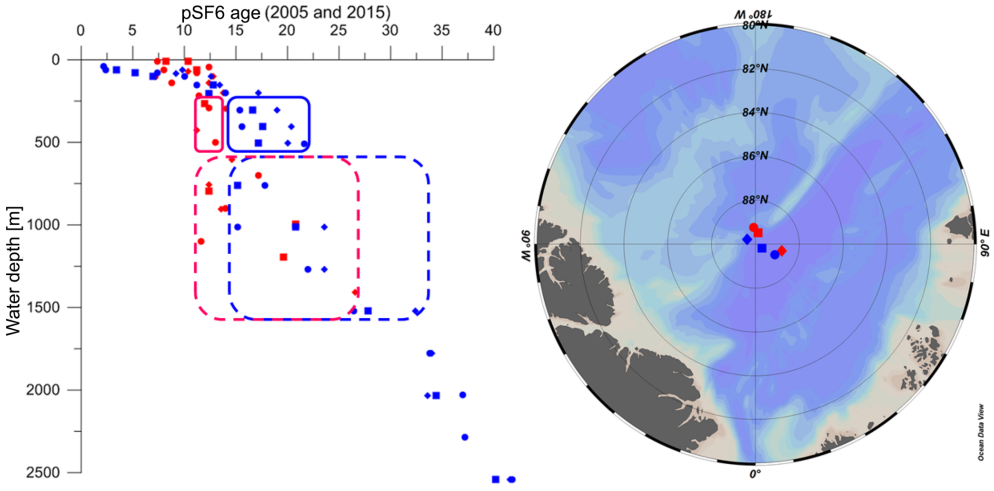

Figure 4. Comparison of pCFC and pSF_6 (partial pressures of CFC and SF6, respectively) ages from 2005 (red) and 2015 (blue) in the Amundsen Basin at stations located in the return flow along the Lomonosov Ridge, distinguishing the depth ranges of FSBW (solid box) and BSBW (dashed box). Locations of 2015 stations are marked in the map as blue symbols (81: dots; 85: squares; 89: diamonds) and 2005 stations in red (41: dots; 42: squares; 46: diamonds). Copyright: Schlitzer, R., Ocean Data View, odv.awi.de (2018).

Anthropogenic tracers can help determine whether the increased Atlantic water contribution had resulted in increased ventilation rates of the intermediate waters in the Amundsen Basin. A comparison of CFC and SF_6 ages between 2005 and 2015 (Fig. 4) shows that both the FSBW (approx. 425 m) and the BSBW (approx. 1025 m) ventilation age did not decrease after 2005. The SF_6 age for the Atlantic Water (BSBW around 1000 m) at the northern end of the section in Fig. 4 is 12–15 years in 2005 and 15–18 years in 2015, suggesting perhaps a slowdown of the transport of Atlantic Water in the boundary current. That would indicate that a change in scavenging along the flow path of the Atlantic water must be responsible for the observed decrease in dissolved ^{230}Th rather than a change in ventilation.

4.4 ^{230}Th removal process in intermediate waters on circulation pathways

In order to judge the scavenging intensity it is useful to compare dissolved ^{230}Th concentrations at various locations along the flow paths of the Atlantic waters. Arctic Intermediate Water (AIW) is comprised of water from the Greenland Sea and the Nordic Seas via the West Spitsbergen Current (WSC) (Rudels, 2009). In the north-east Atlantic at 25° N (GEOTRACES section GA03_W, station 20), dissolved ^{230}Th concentrations are 8.23 fg kg^{-1} at 1000 m and 13.17 fg kg^{-1} at 1500 m (Hayes et al., 2015) (Fig. 5). At 55° N, dissolved ^{230}Th concentrations in 1995 were 3.47 fg kg^{-1} at 500 m and 6.8 fg kg^{-1} at 1625 m (Vogler et al., 1998) (station L3). In the Norwegian Sea, dissolved ^{230}Th concentrations in 1993 were 5.81 fg kg^{-1} at 872 m and 7.04 fg kg^{-1} at 1286 m (Moran et al., 1995) (station 13). These values are above the highest value of dissolved ^{230}Th at 1000 m in the Amundsen Basin in 2015 (5 fg kg^{-1}). That means that these waters have lost ^{230}Th during their transit to the central Amundsen Basin, through the productive North Atlantic and Fram Strait (FSBW) and over the Barents Sea shelf (BSBW). These pathways are influenced by an increased input of terrestrial matter (Günther et al., 2013) and/or increased primary production at the shelf and the ice edge compared to previous years (Arrigo and van Dijken, 2015; Ulfsbo et al., 2018). Relatively high concentrations of Fe at the margin indicate the possibility of enhanced scavenging by iron oxides (Rijkenberg et al., 2018).

At station 400, located at the south-eastern margin of the Eurasian Basin, the deepest water is in the influence of BSBW, downstream of the Barents and Kara Sea shelf and slope. At the largest depth of ∼ 1200 m, the ^{230}Th concentration is low and similar to concentrations in the central Amundsen Basin in 2015. This is consistent with the hypothesis that Atlantic waters that were depleted in ^{230}Th on the shelf contribute to the decrease in dissolved ^{230}Th in the central Amundsen Basin. Such a relic of the scavenging signal implies that scavenging occurs on pathways of inflow waters along the shelves rather than locally within the central basin. The high surface values of dissolved ^{230}Th at station 400 are in line with low export production at this station compared to shallower stations over the shelf (Cai et al., 2010).

Hence, the observed reduction in dissolved ^{230}Th in the intermediate water of the Amundsen Basin is attributed to a combination of scavenging and advection. Scavenging takes place locally on the shelves and along the slopes of the Barents, Kara and Laptev seas, causing the removal of ^{230}Th observed downstream in the central Amundsen Basin. Figure 5 shows pathways of intermediate waters and dissolved ^{230}Th profiles from 2015, illustrating the mechanism controlling

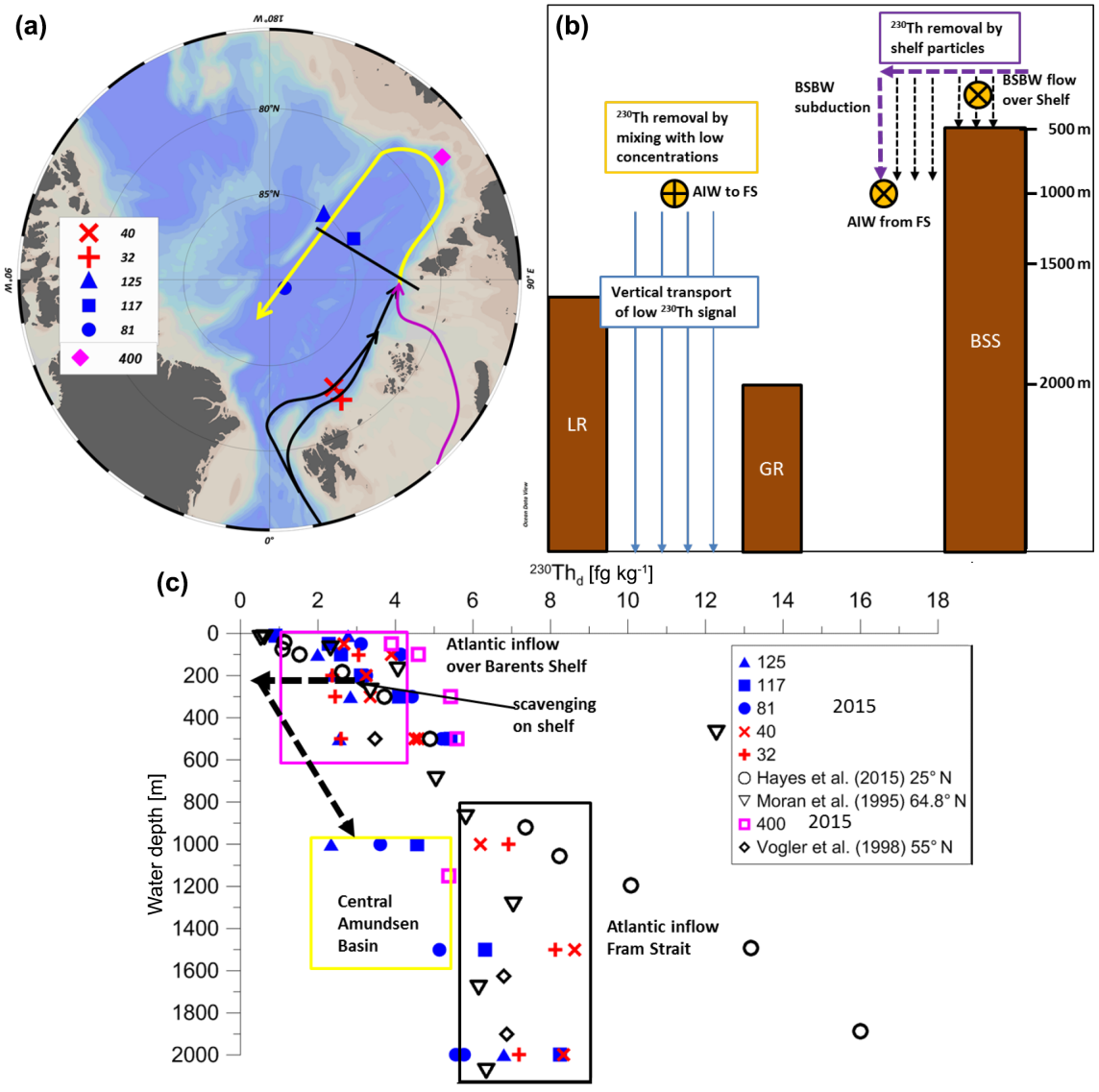

Figure 5. **(a)** Circulation pathways of Atlantic waters to the central Amundsen Basin. **(b)** Conceptual drawing of scavenging and mixing of water masses close to St. Anna Trough (black line in **a** represents the section of **b**). LR: Lomonosov Ridge; GR: Gakkel Ridge; BSS: Barents Sea shelf; FS: Fram Strait. **(c)** Development of dissolved ^{230}Th concentrations from the North Atlantic to the Amundsen Basin. Atlantic values (open symbols; Hayes et al., 2015; Vogler et al., 1998; Moran et al., 1995) are represented by a deep box flowing in through Fram Strait and a shallow box with lower activities flowing in over the Barents Shelf and exposed to additional scavenging on the shelf (horizontal black arrow) before it is subducted and mixed with deeper Atlantic inflow to form the observed reduced concentrations in the central Amundsen Basin. Stations 32 and 40 (red) are from Gdaniec et al. (2020). Copyright: Schlitzer, R., Ocean Data View, odv.awi.de (2018).

the relatively low dissolved ^{230}Th concentrations observed in the central Amundsen Basin. Atlantic waters flowing over the Barents and Kara shelves lose ^{230}Th by increased scavenging. ^{230}Th-depleted BSBW is subducted and gradually mixes with deeper Atlantic inflow. The closer the stations are to the Lomonosov Ridge, the younger the ventilation age (Fig. 5) and the more the salinities are shifted towards Atlantic values. Variability in temperature and salinity plots indicate that this branch interacts with ambient waters (Rudels et al., 1994). This is consistent with dissolved ^{230}Th concentrations observed at stations 81, 117 and 125 (2015), with station 125, located in the TPD and closest to the Lomonosov Ridge, showing the lowest concentrations. The low ^{230}Th concentrations at station 125 may also be affected by additional scavenging due to resuspension on the slope of the Lomonosov Ridge.

4.5 Vertical transport of circulation-derived ^{230}Th scavenging signal and effects in deep waters

Intermediate waters in the central Amundsen Basin have a lower dissolved ^{230}Th in the depth range up to 1500 m due to increased scavenging during the transport of Atlantic water over the shelves and along the slope. The time series data also reveal changing conditions below the intermediate waters, indicated by a decrease in dissolved ^{230}Th in the deeper water column (Fig. 2a).

This raises the question as to whether a change, as observed for 500–1500 m, might cause a decrease in concentrations in the water column below that depth within just 8 years. Theoretically, such a decreasing signal could be manifested by sinking particles via reversible scavenging of sinking particles. With particle settling rates of 582 m yr^{-1} (Rutgers van der Loeff et al., 2018), an average particle needs approximately 6 years from the depth of strongest depletion (1000 m) to reach the bottom of the water column. That would match the timescale of the decrease in ^{230}Th observed between 2007 and 2015. The time for particle transport to depth is the limiting step because the timescale for particle settling is longer than for adsorption and desorption of thorium (Rutgers van der Loeff et al., 2018). On the basis of these parameters, Rutgers van der Loeff et al. (2018) created a model to illustrate the development of ^{228}Ra and ^{228}Th over time. This model is modified here to simulate how the full water column profile of dissolved ^{230}Th in the Amundsen Basin reacts to a sudden change in circulation transport of water with low ^{230}Th into the intermediate depth layer (Table 1). The model should be seen as a description of the downward penetration of the removal signal rather than as a precise retracing of profiles from the central Amundsen Basin. The exchange process used to introduce the ventilated water mass is not meant to reproduce the actual ventilation with water from the Kara or Barents seas, but it merely serves the purpose of creating a rapid reduction in ^{230}Th in the upper 1500 m in order to model the downward propagation of such a signal by reversible scavenging. The model results in Fig. 6 show how fast a decrease in ^{230}Th in the ventilated layer (500–1500 m) is propagated into the deep water. Uncertainties in the model assumptions, such as particle sinking speed and exchange between dissolved and particulate phases, might cause the difference between model and data. This may also explain why the downward penetration of the ventilation signal is slower in the model, where it has not yet reached the seafloor after 8 years (Fig. 6), than in the observed data. But the model results underpin the notion of a dissolved ^{230}Th decrease due to circulation and scavenging along the circulation pathways and account for the reduction in dissolved ^{230}Th below the circulation influence. This temporal change can therefore be explained by a significant reduction in the input of low-^{230}Th waters from shallower depths, even if the scavenging rate in the deep basin remains constant.

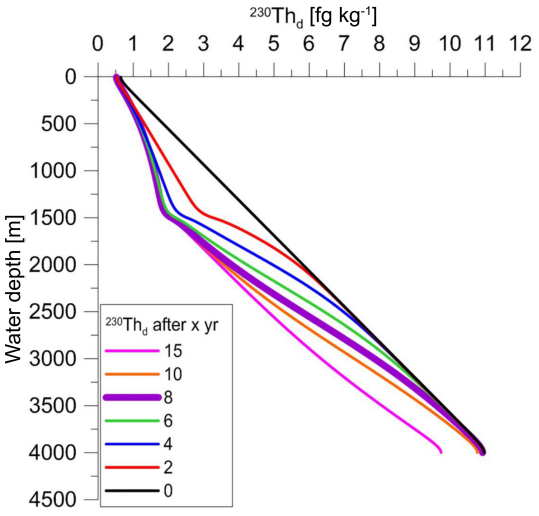

Figure 6. Modelled dissolved ^{230}Th distribution in the Amundsen Basin 0, 2, 4, 6, 8, 10, 15 and 20 years after the reduction in concentration in the upper layer (0–1500 m) by continuous exchange with ^{230}Th-free surface water. The model was modified after Rutgers van der Loeff et al. (2018).

Hydrothermal plumes released by volcanoes at the Gakkel Ridge could also decrease dissolved ^{230}Th efficiently and periodically, as suggested by Valk et al. (2018a) for the deep Nansen Basin. However, these plumes probably do not affect the Amundsen Basin as much as the Nansen Basin due to recirculation in the Nansen Basin that retains most of the hydrothermal-plume-affected waters in the Nansen Basin (Valk et al., 2018a). Additionally, the depths where the major changes occurred in the Amundsen Basin are too shallow (the hydrothermal scavenging starts below 2000 m) and the deep-water decrease in dissolved ^{230}Th in the Amundsen Basin since 2007 is much weaker than in the Nansen Basin (Valk et al., 2018a).

5 Conclusion

Concentrations of dissolved ^{230}Th throughout the entire water column in the Amundsen Basin decreased since 2007. There is no indication of increased scavenging removal of ^{230}Th due to increased particle flux within the Amundsen Basin. An increase in salinity of intermediate water (at 500–1500 m) points to the influence of Atlantic-derived waters, although SF_6 data suggest that the ventilation of this layer has not increased. The reduction in dissolved ^{230}Th concentration in the Amundsen Basin intermediate waters is therefore attributed to increased scavenging from source waters and the transport of this relict scavenging signature by advection. Thus, these downstream waters reflect a scavenging history over the Siberian shelves and slope that results in a reduction in ^{230}Th relative to Atlantic source waters and, in turn, reduced dissolved ^{230}Th in the central Amundsen

Basin. The low-^{230}Th signal is propagated to deeper central Arctic Ocean waters by reversible scavenging. These findings highlight the close interaction of horizontal transport by advection and particle scavenging removal, which combine to generate far-field distributions of reactive trace elements.

Data availability. Data are available at https://doi.org/10.1594/PANGAEA.908068 (Valk et al., 2019) and at https://doi.org/10.1594/PANGAEA.893871 (Valk et al., 2018b.).

Supplement. The supplement related to this article is available online at: https://doi.org/10.5194/os-16-221-2020-supplement.

Author contributions. MMRvdL, OV and WG designed and planned the study. OV, MMRvdL, SG, KL, YL, RP, SBM and VP conducted sampling at sea. RLE and YL analysed the 2007 samples, and OV, VP and SG analysed the 2015 samples. NC provided I/U data; WS provided and interpreted SF_6 data. All authors contributed to writing the paper.

Competing interests. The authors declare that they have no conflict of interest.

Acknowledgements. We thank the captain and crew of RV *Polarstern* for their help during expeditions ARKXXIX/3 and ARKXXII/2. We would like to thank Ronja Paffrath for help on board. Ingrid Stimac is thanked for invaluable technical support and help in the laboratory. This work was partially supported by a U.S. NSF grant (OCE, grant no. 143886) to Robert Lawrence Edwards. Finally we thank the two anonymous reviewers for very thoughtful and constructive comments, which helped to improve the paper.

Financial support. This research has been supported by the NSF (OCE, grant no. 143886) and the Swiss National Science Foundation (AMBIZIONE, grant no. PZ00P2_154805).

The article processing charges for this open-access publication were covered by a Research Centre of the Helmholtz Association.

Review statement. This paper was edited by Matthew Hecht and reviewed by two anonymous referees.

References

Aagaard, K., Coachman, L. K., and Carmack, E. C.: On the halocline of the Arctic Ocean, Deep-Sea Res., 28, 529–545, 1980.

Aagaard, K.: On the deep circulation in the Arctic Ocean, Deep-Sea Res., 28, 251–268, https://doi.org/10.1016/0198-0149(81)90066-2, 1981.

Aksenov, Y., Ivanov, V. V., Nurser, A. J. G., Bacon, S., Polyakov, I. V., Coward, A. C., Naveira-Garabato, A. C., and Beszczynska-Moeller, A.: The Arctic Circumpolar Boundary Current, J. Geophys. Res., 116, C09017, https://doi.org/10.1029/2010JC006637, 2011.

Anderson, R. F., Bacon, M. P., and Brewer, P. G.: Removal of ^{230}Th and ^{231}Pa from the open ocean, Earth Planet. Sc. Lett., 62, 7–23, 1983a.

Anderson, R. F., Bacon, M. P., and Brewer, P. G.: Removal of ^{230}Th and ^{231}Pa at ocean margins, Earth Planet. Sc. Lett., 66, 73–90, 1983b.

Anderson, R. F., Fleisher, M. Q., Robinson, L., Edwards, R. L., Hoff, J. A., Moran, S. B., Rutgers van der Loeff, M. M., Thomas, A. L., Roy-Barman, M., and Francois, R.: GEOTRACES intercalibration of ^{230}Th, ^{232}Th, ^{231}Pa, and prospects for ^{10}Be, Limnol. Oceanogr.-Meth., 10, 179–213, 2012.

Arrigo, K. R. and van Dijken, G. L.: Continued increases in Arctic Ocean primary production, Prog. Oceanogr., 136, 60–70, https://doi.org/10.1016/j.pocean.2015.05.002, 2015.

Arrigo, K. R., van Dijken, G., and Pabi, S.: Impact of a shrinking Arctic ice cover on marine primary production, Geophys. Res. Lett., 35, L19603, https://doi.org/10.1029/2008GL035028, 2008.

Bacon, M. P. and Anderson, R. F.: Distribution of Thorium Isotopes Between Dissolved and Particulate Forms in The Deep Sea, J. Geophys. Res., 87, 2045–2056, 1982.

Bacon, M. P., Huh, C.-A., and Moore, R. M.: Vertical profiles of some natural radionuclides over the Alpha Ridge, Arctic Ocean, Earth Planet. Sc. Lett., 95, 15–22, 1989.

Björk, G., Jakobsson, M., Rudels, B., Swift, J. H., Anderson, L., Darby, D. A., Backman, J., Coakley, B., Winsor, P., Polyak, L., and Edwards, M.: Bathymetry and deep-water exchange across the central Lomonosov Ridge at 88–89° N, Deep-Sea Res. Pt. I, 54, 1197–1208, https://doi.org/10.1016/j.dsr.2007.05.010, 2007.

Björk, G., Anderson, L. G., Jakobsson, M., Antony, D., Eriksson, B., Eriksson, P. B., Hell, B., Hjalmarsson, S., Janzen, T., Jutterström, S., Linders, J., Löwemark, L., Marcussen, C., Anders Olsson, K., Rudels, B., Sellén, E., and Sølvsten, M.: Flow of Canadian basin deep water in the Western Eurasian Basin of the Arctic Ocean, Deep-Sea Res. Pt. I, 57, 577–586, https://doi.org/10.1016/j.dsr.2010.01.006, 2010.

Boetius, A., Albrecht, S., Bakker, K., Bienhold, C., Felden, J., Fernández-Méndez, M., Hendricks, S., Katlein, C., Lalande, C., Krumpen, T., Nicolaus, M., Peeken, I., Rabe, B., Rogacheva, A., Rybakova, E., Somavilla, R., and Wenzhöfer, F.: Export of Algal Biomass from the Melting Arctic Sea Ice, Science, 339, 1430–1432, 2013.

Cai, P., Rutgers van der Loeff, M. M., Stimac, I., Nöthig, E.-M., Lepore, K., and Moran, S. B.: Low export flux of particulate organic carbon in the central Arctic Ocean as revealed by ^{234}Th:^{238}U disequilibrium, J. Geophys. Res., 115, C10037, https://doi.org/10.1029/2009JC005595, 2010.

Casacuberta, N., Christl, M., Vockenhuber, C., Wefing, A.-M., Wacker, L., Masqué, P., Synal, H.-A., and Rutgers van der Lo-

eff, M.: Tracing the Three Atlantic Branches Entering the Arctic Ocean With ^{129}I and ^{236}U, J. Geophys. Res.-Oceans, 123, 6909–6921, https://doi.org/10.1029/2018JC014168, 2018.

Clark, D. L. and Hanson, A.: Central Arctic Ocean Sediment Texture: A Key to Ice Transport Mechanisms, in: Glacial-Marine Sedimentation, edited by: Molnia, B. F., Springer US, Boston, MA, 301–330, 1983.

Cochran, J. K., Hirschberg, D. J., Livingston, H. D., Buesseler, K. O., and Key, R. M.: Natural and anthropogenic radionuclide distributions in the Nansen Basin, Artic Ocean: Scavenging rates and circulation timescales, Deep-Sea Res. Pt. II, 42, 1495–1517, 1995.

Edmonds, H. N., Moran, S. B., Hoff, J. A., Smith, J. R., and Edwards, R. L.: Protactinium-231 and Thorium-230 Abundances and High Scavenging Rates in the Western Arctic Ocean, Science, 280, 405–406, 1998.

Edmonds, H. N., Moran, S. B., Cheng, H., and Edwards, R. L.: ^{230}Th and ^{231}Pa in the Arctic Ocean: implications for particle fluxes and basin-scale Th/Pa fractionation, Earth Planet. Sc. Lett., 227, 155–167, 2004.

Gdaniec, S., Roy-Barman, M., Levier, M., Valk, O., van der Loeff, M. R., Foliot, L., Dapoigny, A., Missiaen, L., Mörth, C.-M., and Andersson, P. S.: ^{231}Pa and ^{230}Th in the Arctic Ocean: Implications for boundary scavenging and ^{231}Pa–^{230}Th fractionation in the Eurasian Basin, Chem. Geol., 532, 119380, https://doi.org/10.1016/j.chemgeo.2019.119380, 2020.

Günther, F., Overduin, P. P., Sandakov, A. V., Grosse, G., and Grigoriev, M. N.: Short- and long-term thermo-erosion of ice-rich permafrost coasts in the Laptev Sea region, Biogeosciences, 10, 4297–4318, https://doi.org/10.5194/bg-10-4297-2013, 2013.

Hansen, R. G. and Ring, E. J.: The preparation and certification of a uranium reference material, Council for Mineral Technology, MINTEK (Analytical Chemistry Divison), Randburg, South Africa, Report, MINTEK-M–84, 12 pp., 1983.

Hayes, C. T., Anderson, R. F., Fleisher, M. Q., Vivancos, S. M., Lam, P. J., Ohnemus, D. C., Huang, K.-F., Robinson, L., Lu, Y., Cheng, H., Edwards, R. L., and Moran, S. B.: Intensity of Th and Pa scavenging partitioned by particle chemistry in the North Atlantic Ocean, Mar. Chem., 170, 49–60, 2015.

Hill, V., Ardyna, M., Lee, S. H., and Varela, D. E.: Decadal trends in phytoplankton production in the Pacific Arctic Region from 1950 to 2012, Deep-Sea Res. Pt. II, 152, 82–94, https://doi.org/10.1016/j.dsr2.2016.12.015, 2017.

Hoffmann, S. S., McManus, J. F., Curry, W. B., and Brown-Leger, S. L.: Persistent export of ^{231}Pa from the deep central Arctic Ocean over the past 35,000 years, Nature, 497, 603–607, 2013.

Hsieh, Y.-T., Henderson, G. M., and Thomas, A. L.: Combining seawater ^{232}Th and ^{230}Th concentrations to determine dust fluxes to the surface ocean, Earth Planet. Sc. Lett., 312, 280–290, 2011.

Jakobsson, M.: Hypsometry and volume of the Arctic Ocean and its constituent seas, Geochem. Geophy. Geosy., 3, 1–18, 2002.

Jones, E. P., Rudels, B., and Anderson, L. G.: Deep waters of the Arctic Ocean: origins and circulation, Deep-Sea Res. Pt. I, 42, 737–760, 1995.

Kanzow, T., von Appen, W.-J., Schaffer, J., Köhn, E., Tsubouchi, T., Wilson, N., Wisotzki, A.: Physical oceanography measured with CTD/Large volume Watersampler-system during POLARSTERN cruise PS100 (ARK-XXX/2), Alfred Wegener Institute, Helmholtz Centre for Polar and Marine Research, Bremerhaven, PANGAEA, https://doi.org/10.1594/PANGAEA.871025, 2017.

Karcher, M., Smith, J. N., Kauker, F., Gerdes, R., and Smethie Jr., W. M.: Recent changes in Arctic Ocean circulation revealed by iodine-129 observations and modeling, J. Geophys. Res., 117, C08007, https://doi.org/10.1029/2011JC007513, 2012.

Kipp, L. E., Charette, M. A., Moore, W. S., Henderson, P. B., and Rigor, I. G.: Increased fluxes of shelf-derived materials to the central Arctic Ocean, Science Advances, 4, eaao1302, https://doi.org/10.1126/sciadv.aao1302, 2018.

Klunder, M. B., Laan, P., Middag, R., de Baar, H. J. W., and Bakker, K.: Dissolved iron in the Arctic Ocean: Important role of hydrothermal sources, shelf input and scavenging removal, J. Geophys. Res., 117, C04014, https://doi.org/10.1029/2011JC007135, 2012.

Middag, R., de Baar, H. J. W., Laan, P., and Bakker, K.: Dissolved aluminium and the silicon cycle in the Arctic Ocean, Mar. Chem., 115, 176–195, https://doi.org/10.1016/j.marchem.2009.08.002, 2009.

Moran, S. B. and Smith, J. N.: ^{234}Th as a tracer of scavenging and particle export in the Beaufort Sea, Cont. Shelf Res., 20, 153–167, https://doi.org/10.1016/S0278-4343(99)00065-5, 2000.

Moran, S. B., Hoff, J. A., Buesseler, K. O., and Edwards, R. L.: High precision ^{230}Th and ^{232}Th in the Norwegian Sea and Denmark by thermal ionization mass spectrometry, Geophys. Res. Lett., 22, 2589–2592, https://doi.org/10.1029/95GL02652, 1995.

Moran, S. B., Shen, C.-C., Edwards, R. L., Edmonds, H. N., Scholten, J. C., Smith, J. N., and Ku, T.-L.: ^{231}Pa and ^{230}Th in surface sediments of the Arctic Ocean: Implications for ^{231}Pa/^{230}Th fractionation, boundary scavenging, and advective export, Earth Planet. Sc. Lett., 234, 235–248, 2005.

Nozaki, Y., Horibe, Y., and Tsubota, H.: The water column distributions of thorium isotopes in the western North Pacific, Earth Planet. Sc. Lett., 54, 203–216, https://doi.org/10.1016/0012-821X(81)90004-2, 1981.

Pabi, S., van Dijken, G. L., and Arrigo, K. R.: Primary production in the Arctic Ocean, 1998–2006, J. Geophys. Res., 113, C08005, https://doi.org/10.1029/2007JC004578, 2008.

Polyakov, I. V., Pnyushkov, A. V., Alkire, M. B., Ashik, I. M., Baumann, T. M., Carmack, E. C., Goszczko, I., Guthrie, J., Ivanov, V. V., Kanzow, T., Krishfield, R., Kwok, R., Sundfjord, A., Morison, J., Rember, R., and Yulin, A.: Greater role for Atlantic inflows on sea-ice loss in the Eurasian Basin of the Arctic Ocean, Science, 356, 285–291, https://doi.org/10.1126/science.aai8204, 2017.

Owens, S. A., Buesseler, K. O., and Sims, K. W. W.: Re-evaluating the ^{238}U-salinity relationship in seawater: Implications for the ^{238}U–^{234}Th disequilibrium method, Mar. Chem., 127, 31–39, 2011.

Rabe, B., Karcher, M., Kauker, F., Schauer, U., Toole, J. M., Krishfield, R. A., Pisarev, S., Kikuchi, T., and Su, J.: Arctic Ocean basin liquid freshwater storage trend 1992–2012, Geophys. Res. Lett., 41, 961–968, https://doi.org/10.1002/2013GL058121, 2014.

Rabe, B., Schauer, U., Ober, S., Horn, M., Hoppmann, M., Korhonen, M., Pisarev, S., Hampe, H., Villacieros, N., Savy, J. P., and Wisotzki, A.: Physical oceanography during POLARSTERN cruise PS94 (ARK-XXIX/3), Alfred Wegener Institute, Helmholtz Center for Polar and Marine Research, Bremer-

haven, PANGAEA, https://doi.org/10.1594/PANGAEA.859558, 2016.

Rempfer, J., Stocker, T. F., Joos, F., Lippold, J., and Jaccard, S. L.: New insights into cycling of ^{231}Pa and ^{230}Th in the Atlantic Ocean, Earth Planet. Sc. Lett., 468, 27–37, https://doi.org/10.1016/j.epsl.2017.03.027, 2017.

Rijkenberg, M. J. A., Slagter, H. A., Rutgers van der Loeff, M., van Ooijen, J., and Gerringa, L. J. A.: Dissolved Fe in the Deep and Upper Arctic Ocean With a Focus on Fe Limitation in the Nansen Basin, Frontiers in Marine Science, 5, 88, https://doi.org/10.3389/fmars.2018.00088, 2018.

Roy-Barman, M.: Modelling the effect of boundary scavenging on Thorium and Protactinium profiles in the ocean, Biogeosciences, 6, 3091–3107, https://doi.org/10.5194/bg-6-3091-2009, 2009.

Roy-Barman, M., Lemaître, C., Ayrault, S., Jeandel, C., Souhaut, M., and Miquel, J. C.: The influence of particle composition on Thorium scavenging in the Mediterranean Sea, Earth Planet. Sc. Lett., 286, 526–534, 2009.

Rudels, B.: Arctic Ocean Circulation, in: Encyclopedia of Ocean Sciences, 2nd edn., edited by: Steele, J. H., Academic Press, Oxford, 211–225, 2009.

Rudels, B.: Physical oceanography during ODEN cruise OD91, PANGAEA, https://doi.org/10.1594/PANGAEA.742746, 2010.

Rudels, B.: Arctic Ocean circulation and variability – advection and external forcing encounter constraints and local processes, Ocean Sci., 8, 261–286, https://doi.org/10.5194/os-8-261-2012, 2012.

Rudels, B., Jones, E. P., Anderson, L. G., and Kattner, G.: On the Intermediate Depth Waters of the Arctic Ocean, in: The Polar Oceans and Their Role in Shaping the Global Environment, edited by: Johannessen, O. M., Muench, R. D., and Overland, J. E., AGU, 33–46, 1994.

Rudels, B., Schauer, U., Björk, G., Korhonen, M., Pisarev, S., Rabe, B., and Wisotzki, A.: Observations of water masses and circulation with focus on the Eurasian Basin of the Arctic Ocean from the 1990s to the late 2000s, Ocean Sci., 9, 147–169, https://doi.org/10.5194/os-9-147-2013, 2013.

Rudels, B., Korhonen, M., Schauer, U., Pisarev, S., Rabe, B., and Wisotzki, A.: Circulation and transformation of Atlantic water in the Eurasian Basin and the contribution of the Fram Strait inflow branch to the Arctic Ocean heat budget, Prog. Oceanogr., 132, 128–152, https://doi.org/10.1016/j.pocean.2014.04.003, 2015.

Rutgers van der Loeff, M. M. and Berger, G. W.: Scavenging of ^{230}Th and ^{231}Pa near the Antarctic Polar Front in the South Atlantic, Deep-Sea Res. Pt. I, 40, 339–357, 1993.

Rutgers van der Loeff, M. M., Key, R. M., Scholten, J., Bauch, D., and Michel, A.: ^{228}Ra as a tracer for shelf water in the Arctic Ocean, Deep-Sea Res. Pt. II, 42, 1533–1553, 1995.

Rutgers van der Loeff, M., Kipp, L., Charette, M. A., Moore, W. S., Black, E., Stimac, I., Charkin, A., Bauch, D., Valk, O., Karcher, M., Krumpen, T., Casacuberta, N., Smethie, W., and Rember, R.: Radium Isotopes Across the Arctic Ocean Show Time Scales of Water Mass Ventilation and Increasing Shelf Inputs, J. Geophys. Res.-Oceans, 123, 4853–4873, https://doi.org/10.1029/2018JC013888, 2018.

Schauer, U. and Wisotzki, A.: Physical oceanography during POLARSTERN cruise ARK-XXII/2 (SPACE), PANGAEA, https://doi.org/10.1594/PANGAEA.733418, 2010.

Schlitzer, R.: Ocean Data View, available at: https://odv.awi.de (last access: November 2019), 2018.

Scholten, J. C., Rutgers van der Loeff, M. M., and Michel, A.: Distribution of ^{230}Th and ^{231}Pa in the water column in relation to the ventilation of the deep Arctic basins, Deep-Sea Res. Pt. II, 42, 1519–1531, 1995.

Schuur, E. A. G., Abbott, B. W., Bowden, W. B., Brovkin, V., Camill, P., Canadell, J. G., Chanton, J. P., Chapin, F. S., Christensen, T. R., Ciais, P., Crosby, B. T., Czimczik, C. I., Grosse, G., Harden, J., Hayes, D. J., Hugelius, G., Jastrow, J. D., Jones, J. B., Kleinen, T., Koven, C. D., Krinner, G., Kuhry, P., Lawrence, D. M., McGuire, A. D., Natali, S. M., O'Donnell, J. A., Ping, C. L., Riley, W. J., Rinke, A., Romanovsky, V. E., Sannel, A. B. K., Schädel, C., Schaefer, K., Sky, J., Subin, Z. M., Tarnocai, C., Turetsky, M. R., Waldrop, M. P., Walter Anthony, K. M., Wickland, K. P., Wilson, C. J., and Zimov, S. A.: Expert assessment of vulnerability of permafrost carbon to climate change, Climatic Change, 119, 359–374, https://doi.org/10.1007/s10584-013-0730-7, 2013.

Schuur, E. A. G., McGuire, A. D., Schädel, C., Grosse, G., Harden, W. J., Hayes, D. J., Hugelius, G., Koven, C. D., Kuhry, P., Lawrence, D. M., Natali, S. M., Olefeldt, D., Romanovsky, V. E., Schaefer, K., Turetsky, M. R., Treat, C. C., and Vonk, J. E.: Climate change and the permafrost carbon feedback, Nature, 520, 171–179, 2015.

Serreze, M. C. and Stroeve, J.: Arctic sea ice trends, variability and implications for seasonal ice forecasting, Philos. T. Roy. Soc. A, 373, 20140159, https://doi.org/10.1098/rsta.2014.0159, 2015.

Serreze, M. C., Stroeve, J., Barrett, A. P., and Boisvert, L. N.: Summer atmospheric circulation anomalies over the Arctic Ocean and their influences on September sea ice extent: A cautionary tale, J. Geophys. Res.-Atmos., 121, 11463–11485, https://doi.org/10.1002/2016JD025161, 2016.

Shen, C.-C., Cheng, H., Edwards, R. L., Moran, S. B., Edmonds, H. N., Hoff, J. A., and Thomas, R. B.: Measurement of Attogram Quantities of ^{231}Pa in Dissolved and Particulate Fractions of Seawater by Isotope Dilution Thermal Ionization Mass Spectroscopy, Anal. Chem., 75, 1075–1079, https://doi.org/10.1021/ac026247r, 2003.

Slagter, H. A., Reader, H. E., Rijkenberg, M. J. A., Rutgers van der Loeff, M., de Baar, H. J. W., and Gerringa, L. J. A.: Organic Fe speciation in the Eurasian Basins of the Arctic Ocean and its relation to terrestrial DOM, Mar. Chem., 197, 11–25, https://doi.org/10.1016/j.marchem.2017.10.005, 2017.

Tanhua, T., Jones, E. P., Jeansson, E., Jutterström, S., Smethie, W. M., Wallace, D. W. R., and Anderson, L. G.: Ventilation of the Arctic Ocean: Mean ages and inventories of anthropogenic CO_2 and CFC-11, J. Geophys. Res., 114, C01002, https://doi.org/10.1029/2008JC004868, 2009.

Trimble, S. M., Baskaran, M., and Porcelli, D.: Scavenging of thorium isotopes in the Canada Basin of the Arctic Ocean, Earth Planet. Sc. Lett., 222, 915–932, 2004.

Ulfsbo, A., Cassar, N., Korhonen, M., van Heuven, S., Hoppema, M., Kattner, G., and Anderson, L. G.: Late summer net community production in the central Arctic Ocean using multiple approaches, Global Biogeochem. Cy., 28, 1129–1148, https://doi.org/10.1002/2014GB004833, 2014.

Ulfsbo, A., Jones, E. M., Casacuberta, N., Korhonen, M., Rabe, B., Karcher, M., and van Heuven, S. M. A. C.: Rapid changes in anthropogenic carbon storage and ocean acidification in the intermediate layers of the Eurasian Arctic Ocean:

1996–2015, Global Biogeochemical Cycles, 32, 1254–1275, https://doi.org/10.1029/2017GB005738, 2018.

Valk, O., Rutgers van der Loeff, M. M., Geibert, W., Gdaniec, S., Rijkenberg, M. J. A., Moran, S. B., Lepore, K., Edwards, R. L., Lu, Y., and Puigcorbé, V.: Importance of Hydrothermal Vents in Scavenging Removal of ^{230}Th in the Nansen Basin, Geophys. Res. Lett., 45, 10539–10548, https://doi.org/10.1029/2018GL079829, 2018.

Valk, O., Rutgers van der Loeff, M. M., and Geibert, W.: Thorium isotopes in the water column in Nansen Basin during POLARSTERN cruises PS70 (ARK-XXII/2) in 2007 and PS94 (ARK-XXIX/3) in 2015, PANGAEA, https://doi.org/10.1594/PANGAEA.893871, 2018b.

Valk, O., Rutgers van der Loeff, M. M., Geibert, W., Gdaniec, S., Moran, S. B., Lepore, K., Edwards, R. L., Lu, Y., Puigcorbé, V., Casacuberta, N., Paffrath, R., Smethie, W., and Roy-Barman, M.: Thorium isotopes in the water column in Amundsen Basin during POLARSTERN cruises PS70 (ARK-XXII/2) in 2007 and PS94 (ARK-XXIX/3) in 2015, PANGAEA, https://doi.org/10.1594/PANGAEA.908068, 2019.

Vogler, S., Scholten, J., Rutgers van der Loeff, M., and Mangini, A.: ^{230}Th in the eastern North Atlantic: the importance of water mass ventilation in the balance of ^{230}Th, Earth Planet. Sc. Lett., 156, 61–74, https://doi.org/10.1016/S0012-821X(98)00011-9, 1998.

Wang, Q., Wekerle, C., Danilov, S., Koldunov, N., Sidorenko, D., Sein, D., Rabe, B., and Jung, T.: Arctic Sea Ice Decline Significantly Contributed to the Unprecedented Liquid Freshwater Accumulation in the Beaufort Gyre of the Arctic Ocean, Geophys. Res. Lett., 45, 4956–4964, https://doi.org/10.1029/2018GL077901, 2018.

Wheeler, P. A., Watkins, J. M., and Hansing, R. L.: Nutrients, organic carbon and organic nitrogen in the upper water column of the Arctic Ocean: implications for the sources of dissolved organic carbon, Deep Sea Res. Pt. II, 44, 1571–1592, https://doi.org/10.1016/S0967-0645(97)00051-9, 1997.

Worthington, L. V.: Oceanographic results of project Skijump I and Skijump II in the Polar Sea, 1951–1952, Eos T. Am. Geophys. Un., 34, 543–551, https://doi.org/10.1029/TR034i004p00543, 1953.